Apr 21st, 12:40 PM - 1:40 PM

Application of Wray-Agarwal Turbulence Model to Axisymmetric Subsonic and Transonic Flows

Mike Kiely
Washington University in St. Louis

Application of Wray-Agarwal Turbulence Model to Axisymmetric Subsonic and Transonic Flows

Mike Kiely
Washington University in St. Louis
Dr. Ramesh Agarwal

Abstract

This paper describes the problem setup, implementation, and numerical results obtained with the commercial CFD software ANSYS Fluent to test the accuracy of the one-equation Wray-Agarwal (WA) turbulence model in comparison to the commonly used one-equation Spalart-Allmaras (SA) turbulence model by computing two axisymmetric benchmark problems, namely the subsonic flow past an axisymmetric after-body and the transonic flow past Sandia axisymmetric bump. The axisymmetric after-body case features low speed flow in near separation conditions where it was found that the Wray-Agarwal model and the Spalart-Allmaras model produced nearly identical results. The Sandia transonic axisymmetric bump case features a complex flow in which shock induced separation occurs over the geometry. In this test case the Wray-Agarwal model was seen to improve accuracy over the Spalart-Allmaras model in terms of pressure distribution and separation prediction on the bump.

Introduction

The Wray-Agarwal (WA) Model is a recently developed one-equation linear eddy viscosity model which has been shown in several test cases to improve solution accuracy over the widely used Spalart-Allmaras (SA) model [1]. This paper details the problem set up and numerical simulation of two axisymmetric turbulence modelling benchmark test cases using the WA and SA turbulence models for purpose of validation and comparison of results. The first case tested was a low speed, axisymmetric afterbody case [2]. Results for this case were compared to results obtained by NASA using several solvers and turbulence models. In this case the WA Model was seen to produce relatively similar predictions to the SA model. A second axisymmetric test case was performed in the Sandia transonic axisymmetric bump case in which predictions from both models were compared to experimentally published data. In this case, the WA model was seen to provide much more accurate results in the prediction of the formation of a shock induced separation zone.

Numerical Methods

Both test cases were calculated using pressure based, steady state RANS equations solvers in Ansys Fluent. Air in both cases was assumed to follow the ideal gas law as well as Sutherland's law for viscosity. The solver used the simple algorithm for pressure-velocity coupling, second order upwind schemes for all convection terms, and central differencing for viscous terms. Both the SA and the WA turbulence model were tested for both cases.

Spalart-Allmaras Turbulence Model

The Spalart-Allmaras (SA) turbulence model is widely used one equation turbulence model. The SA Model is a linear eddy viscosity model which employs Boussinesq's assumption to solve for turbulent shear stress [2]. Having only one transport equation, the SA model does not account for

turbulent kinetic energy in its solution to flows. The SA model has been shown to be fairly accurate for wall bounded flows with regions of separation.

Wray-Agarwal Turbulence Model

The Wray-Agarwal (WA) model is a one equation linear eddy viscosity turbulence model which similarly employs the Boussinesq assumption to solve for turbulent shear stresses. The WA model was originally derived from the k-ω closure model and contains a switching function function to allow it to behave similar to a k-ε in the farfield and a k-ω model near walls. The WA model in the past has been shown to improve accuracy from the SA model and give results which are competitive with the k-ω model in a variety of flows.

Axisymmetric Afterbody Test Case

The Axisymmetric afterbody case was originally created by NASA in 2017 as a turbulence modelling validation case [2]. This case was designed to feature precise areas near separation at low speed flows in order to test models' ability to predict these effects. Experimental wind tunnel data has not yet been gathered for this geometry.

Geometry

The geometry of this test case is a curve driven axisymmetric body containing 4 separate sections, as seen below in Fig 1.

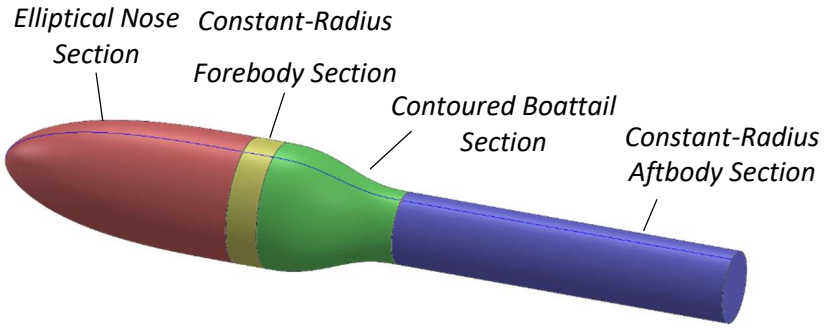

Figure 1: Geometry of axisymmetric afterbody

Each section of the model in Fig. 1 is described by a curve along the x plane. The definition of the elliptical nose section is given in Eq. (2).

$$R(x) = r_1\left(1 - \frac{x + L_F + L_N}{L_N}\right) + r_2\left(\frac{x + L_F + L_N}{L_N}\right) \; ; \; -(L_F + L_N) \leq x \leq -L_F \tag{1}$$

with

$$r_1 = R_{max}\left[1 - \left(\frac{x + L_F}{L_N}\right)^2\right]^{\frac{1}{2}} \tag{1a}$$

$$r_2 = R_{max}\left[1 - \left(\frac{x + L_F}{L_N}\right)^4\right]^{\frac{1}{4}} \quad (1b)$$

where R_{max} denotes the maximum radius of the body, and L_N and L_F denote the length of the body's nose and forebody section respectively. The equation describing the radius at the constant radius fore-body section in Fig. 1 is given as follows.

$$R(x) = R_{max}\ ;\ -L_F \leq x \leq 0 \quad (2)$$

The curve describing the contoured boattail section is given in Eq. (3).

$$R(x) = a_1 + a_2x^3 + a_3x^4 + a_4x^5\ ;\ 0 \leq x \leq L_B \quad (3)$$

with

$$a_1 = R_{max} \quad (3a)$$

$$a_2 = \frac{-10R_{max}(1-\sigma)}{L_B^3} \quad (3b)$$

$$a_3 = \frac{15R_{max}(1-\sigma)}{L_B^4} \quad (3c)$$

$$a_4 = \frac{-6R_{max}(1-\sigma)}{L_B^5} \quad (3d)$$

where σ denotes the ratio of the minimum and maximum radius of the body and L_B denots the length of the boattail section. The constant radius aft-body section is defined as follows in Eq. (4).

$$R(x) = \sigma R_{max}\ ;\ L_B \leq x \leq (L_B + L_A) \quad (4)$$

where L_A denotes the length of the constant radius aftbody section. The specific geometric parameters used in Eqs. (1) – (4) are given in Table 1.

Table 1: Geometric parameters used in the test case

Parameter	Value
R_{max}	3 in.
L_N	4 R_{max}
L_F	0.5 R_{max}
L_B	2.1 R_{max}
L_A	5.5 R_{max}
σ	0.575

Computational Set Up

The simulations were run to match the NASA specified flow conditions. A pressure far field boundary condition was used with a freestream velocity of 40 m/s at the inlet resulting in a Reynolds number based on the maximum radius of the body of 180,000. The body was assumed to have a no slip wall boundary condition as well as the walls of the 15 inch square wind tunnel. At the outflow of the tunnel a static pressure ratio (p/p_∞) of 0.998 was maintained to ensure an inflow Mach Number of 0.117. The axisymmetric nature of this case allowed for a smaller cross section of the overall geometry to be considered. A 1 degree revolution of the geometry was modeled in accordance with the NASA experiment [2]. Symmetry boundary conditions were enforced on the side planes of the flow domain.

Use of the 1-degree revolution of the geometry allowed for a highly refined mesh at a lesser computational cost. The flow domain extended 55 inches upstream of the nose of the body. A total of 350 streamwise grid divisions were used along the profile of the body in the streamwise direction with the upstream component of the wind tunnel containing 150 grid divisions. Normal to the surface of the body, 200 grid points were employed leading to a maximum y+ value in the boundary layer of 0.15. The computational domain and mesh are shown in Fig. 2.

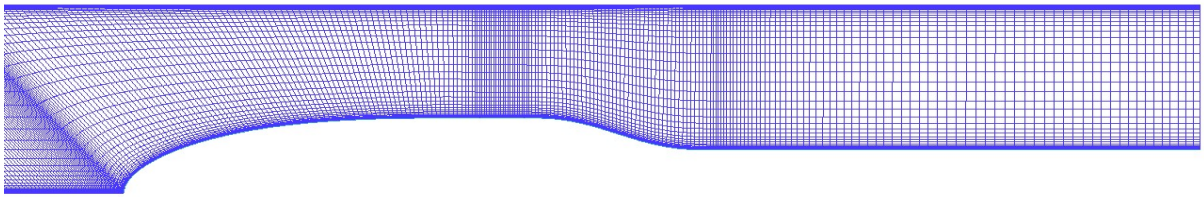

Figure 2: Computational domain and mesh around the axisymmetric body

Numerical simulations were performed using a pressure-based Reynolds-Averaged Navier-Stokes (RANS) equations solver in ANSYS Fluent with Spalart-Allmaras (SA) and Wray-Agarwal (WA) turbulence models.

Results

The simulation results for this test case using the SA and WA turbulence models were almost the same and matched well with the NASA reported results. The computed Mach number contours in the flow domain using the two turbulence models are shown in Fig. 3.

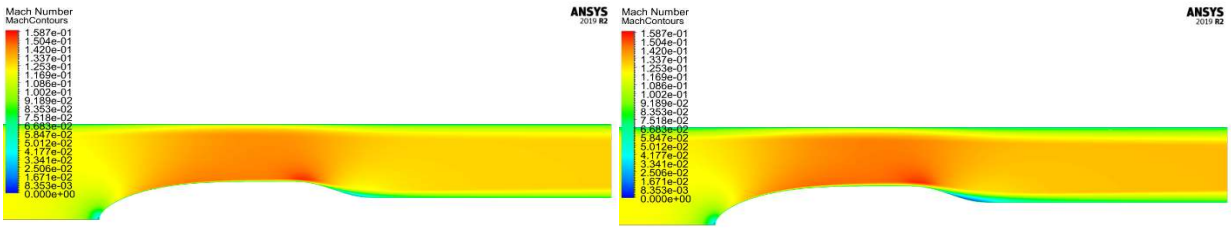

(a) SA Model **(b) WA Model**

Figure 3: Mach number contours around the axisymmetric body

In Fig. 3, a small deviation can be seen between the results from the two turbulence models; the WA model seems to predict a slightly more pronounced separated flow region compared to SA model along the boattail section. Figures 4 and 5 show the pressure distribution and skin-friction on the body respectively; it can be seen that both SA and WA model give almost identical results. Comparing to NASA's published results, both the SA model with curvature correction and the SST k- ω model predict flow with hardly noticeable separation region with identifiable separation and reattachment points [2]. In this low speed nearly separated flow in the boattail region, the WA model is found to predict the flow field close to that predicted by the standard SA model (without curvature effect) and the k-kL two-equation model [3]. An important point to note is that since this case has not been tested in the wind tunnel; exact nature of the flow field in the bottail region cannot be specified with certainty based only on the computational results.

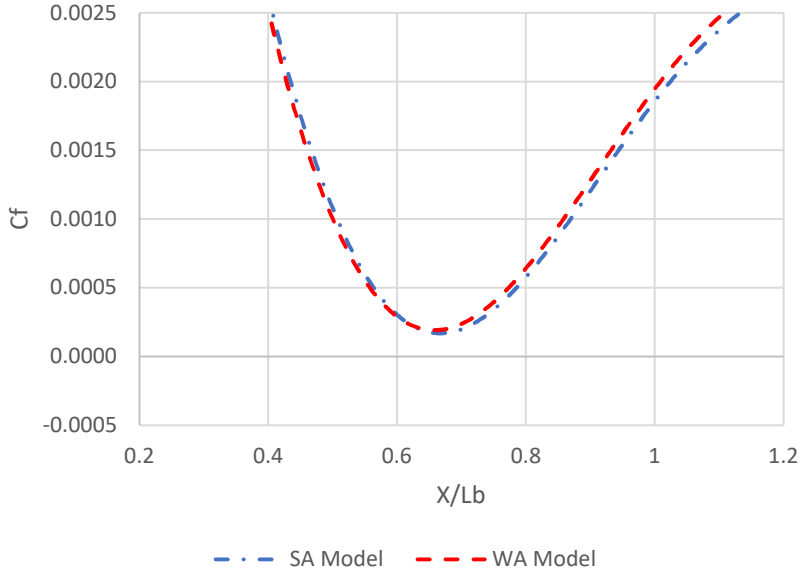

Figure 4: Pressure coefficient on the boattail section of the axisymmetric body

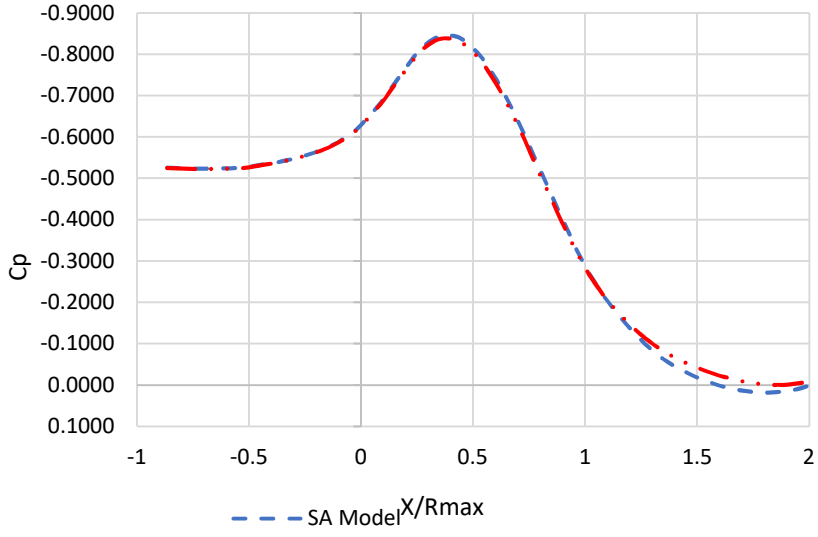

Figure 5: Skin-friction coefficient on the boattail section of the axisymmetric body

Axisymmetric Transonic Bump

Another benchmark test case considered in this paper is an axisymmetric transonic bump; it was run to evaluate the relative accuracy of SA and WA models in predicting flows experiencing shock induced separation in transonic flow. This case is based on an experiment of Bachalo and Johnson in March 1986 [4]; it was issued as a CFD challenge by Sandia labs in 2019 due to the complexity of its flow field [5].

Geometry

The axisymmetric bump tested by Sandia labs consists of a scaled down version of the original geometry of Bachalo and Johnson [5]. This geometry consists of a cylindrical body with an elliptical nose section and a bump. A cross sectional diagram of the geometry is shown in Fig. 5.

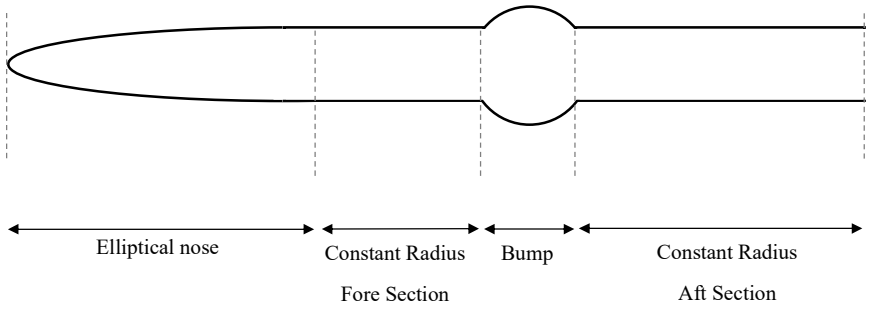

Figure 5: Cross sectional diagram of Sandia transonic axisymmetric bump

In the scaled down model shown in Fig. 5, the diameter of the cylinder is 1.9 inches and the characteristic chord length of the bump is 2.53 inches. The total thickness of the bump is 0.75 inches. A leading edge fillet on the fore section of the bump is used with radius of 2.23 inches; however experiments in the past have pointed that this fillet has negligible effect on flow behavior [3]. In order to determine the effects of the turbulence models on prediction of shock induced separation on the bump and to simplify the simulations, the elliptical nose of the geometry is not included in the computations. Since the nose was designed to minimize the shock effects, this simplification is found to provide reasonably close description of the bump flow field so long as the constant radius section fore of the bump was long enough to produce fully developed flow downstream. The full tested geometry is shown in Fig. 6.

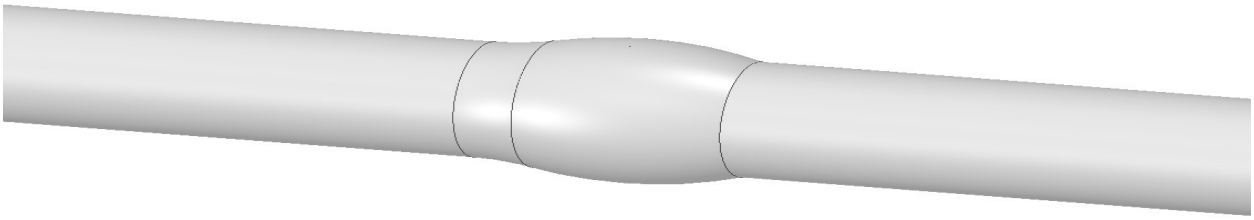

Figure 6: Sandia geometry of transonic bump

Computational Setup

The computational domain for this case is extended 3.3 chord lengths upstream and 4.4 chord lengths downstream of the bump. In the z direction, the domain extended 12 inches to match the original flow conditions in Sandia's 1x1 transonic wind tunnel. Being an axisymmetric case, a 1 degree rotation about the x axis is used for further simplification in simulations, similar to the previous case of subsonic flow over a boattail. A series of meshes were generated to conduct a grid dependence of solution study. Based on this study, the finest mesh which included 1400 divisions in the stream-wise directions and 700 divisions in the direction normal to the surface with a maximum y+ value in the boundary layer of 0.15 was used in the simulations reported in this paper for this test case. A coarsened image of the mesh is shown in Fig. 7.

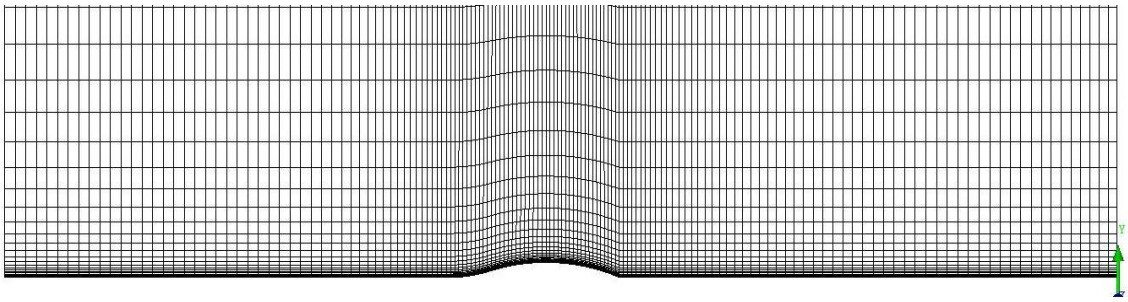

Figure 7: Coarse grid structured volume mesh for the Sandia transonic bump

In keeping with the original experiment, this case was run at a Mach number of 0.875. A ratio of static to total pressure at the inlet was employed as a boundary condition to maintain this freestream Mach number. For the WA turbulence model, a freestream value for the variable R (turbulent eddy viscosity) was chosen to be 4 times the freestream dynamic viscosity. Several simulations were run to evaluate the sensitivity of the solution to both grid refinement and boundary conditions, particularly in the region just downwind of the bump. As mentioned before, all results shown in this paper were obtained on the finest grid and are mesh independent. The boundary conditions were chosen to represent the experimental value including the stagnation temperature of 318 K and total back pressure to total free stream pressure ratio of 0.5825.

Results

Both the WA and SA model are found to predict the onset of shock induced separation correctly. Also, outside or away from the shock induced separation zone, the results from the two models are close; however the differences arise in the separation region as can be seen in Fig. 8.

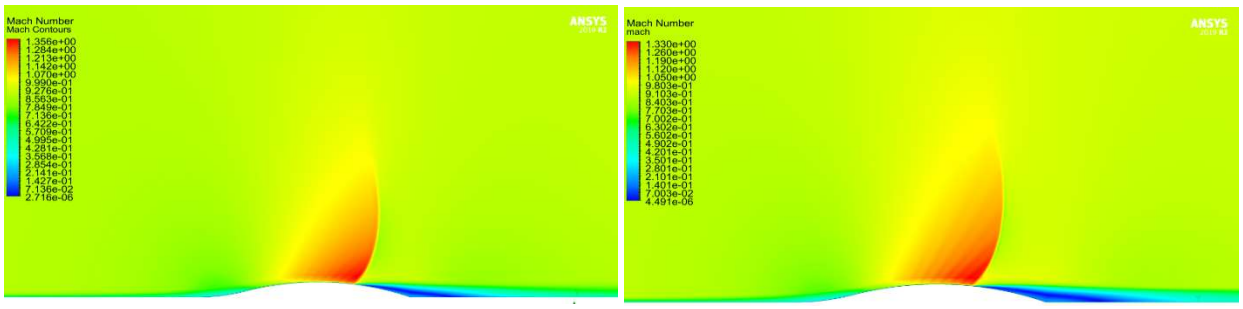

(a) SA Model **(b) WA Model**

Figure 8: Mach number contours and shock wave formation on axisymmetric transonic bump

The WA model predicts a slightly earlier shock formation and separation zone than the SA model. This effect can further be seen by examining both the pressure coefficient and the skin friction coefficient over the surface of the bump within the separation zone in Fig. 9 and Fig. 10 respectively.

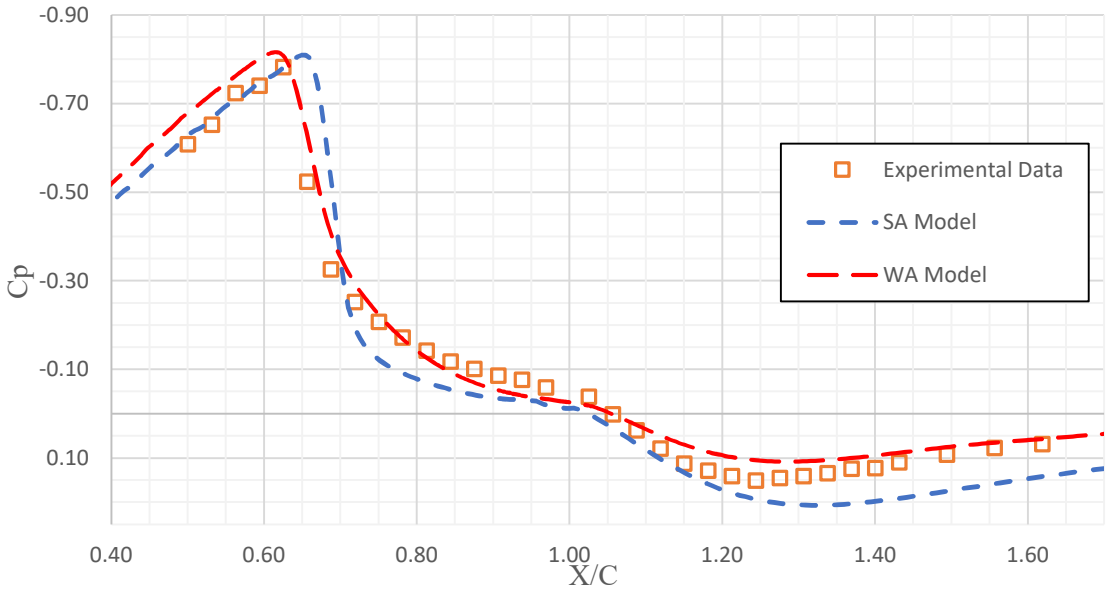

Figure 9: Pressure coefficient distribution on the axisymmetric bump

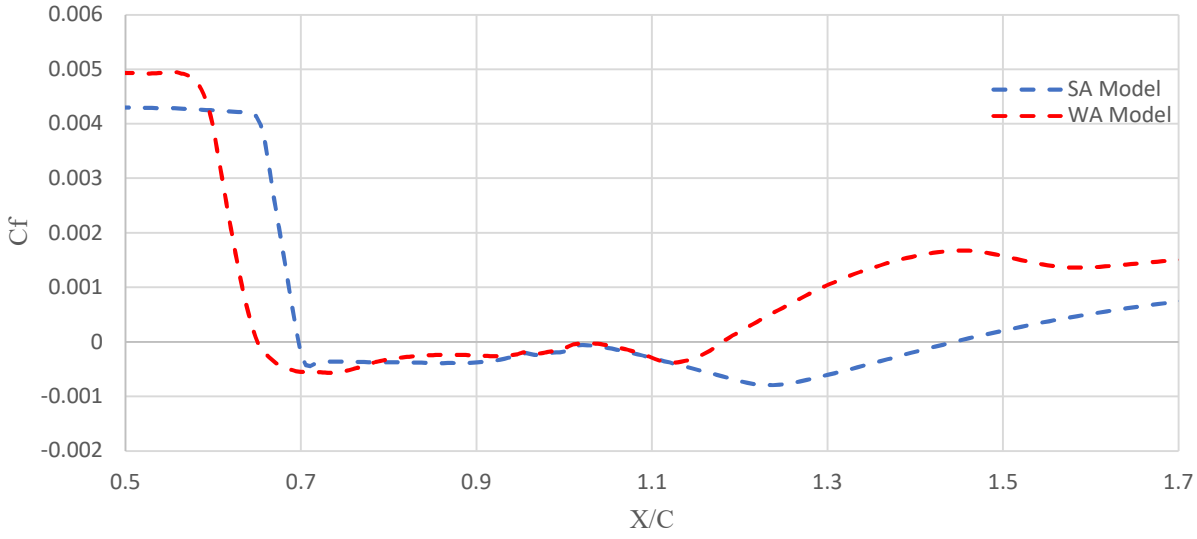

Figure 10: Skin friction coefficient distribution on the axisymmetric bump

From Figs. 8-10, it can be seen that the formation of the shockwave is predicted by both turbulence models around x/c = 0.65. Consequently, the onset of separation, defined by a negative skin friction coefficient value, can be seen from Fig. 10 to occur shortly after. As can be seen in Table 2, the separation length prediction by the WA model is much closer to the

experimental value compared to that predicted by the SA model. The WA model predicts the onset of separation slightly early; however overall the prediction of separation region by WA model is much closer to experimental value. Additionally, as shown in Fig. 8, the WA model predicts the pressure coefficient distribution on the bump to a higher degree of accuracy than the SA model.

Table 2: Separation predictions from SA and WA turbulence models compared to experimental data

	x/c at Separation	x/c at Reattachment	Separation Length
SA Model	0.70	1.47	0.77
WA Model	0.66	1.20	0.54
Experimental	0.68	1.19	0.51

Conclusions

In this paper, the results of the two turbulence modeling benchmark test cases, namely the subsonic flow past an axisymmetric after-body and the Sandia transonic bump are presented using the Wray-Agarwal (WA) and the Spalart-Allmaras (SA) models. In the axisymmetric afterbody test case, the results from WA model and SA model are almost identical. However, in the Sandia transonic axisymmetric bump test case, the WA model is found to produce results in much closer agreement to the experimental data than the SA model for both pressure distribution and separation prediction. Overall, it has been demonstrated that the WA model can improve accuracy of turbulent flow simulations compared to the SA model for transonic flow cases that include separation due to shock/boundary layer interaction.

Acknowledgement

Funding for this project was provided by MO NASA Space Grant Consortium Grant Award number 80NSSC20M0100.

Biography

Mike is a PhD student at Washington University. He received his Bachelor's degree in aerospace engineering from Missouri University of Science in Technology in 2020. Mike's past research involves computational fluid dynamics and turbulence modelling. His current research is focused on multidisciplinary design optimization using multi fidelity CFD, with specific applications to hydrogen powered, emission free commercial airliners. Upon graduation, Mike hopes to continue his work in the field of green aviation.

References

1. Han, X., Rahman, M., and Agarwal, R. K., "Development and Application of Wall-Distance-Free Wray-Agarwal Turbulence Model (WA2018)," AIAA Paper 2018-0593, AIAA Aerospace Sciences Meeting, 2018.

2. Disotell, K. J., and Rumsey, C. L., “Development of an Axisymmetric Afterbody Test Case for Turbulent Flow Separation Validation,” NASA TM-2017-219680, January 2017.

3. NASA Langley Research Center Turbulence Modelling Resource, available: https://turbmodels.larc.nasa.gov/index.html.

4. Bachalo, W.D., and Johnson, D. A., "Transonic, Turbulent Boundary-Layer Separation Generated on an Axisymmetric Flow Model," AIAA J., 1986, pp. 437-443.

5. Beresh, S. J., Barone, M. F., Dowding, K. J., Lynch, K. P., Miller, N. E., and Lance, B. W., "A CFD Validation Challenge for Transonic, Shock-Induced Separated Flow: Approach and Metrics," AIAA Paper 2020-1308, January 2020, https://doi.org/10.2514/6.2020-1308.